Pharm Res (2015) 32:196–210
DOI 10.1007/s11095-014-1455-7

RESEARCH ARTICLE

Star-Shaped Tetraspermine Enhances Cellular Uptake and Cytotoxicity of T-Oligo in Prostate Cancer Cells

Vidula Kolhatkar • Hiren Khambati • Asawari Lote • Peter Shanine • Thomas Insley • Soumyo Sen • Gnanasekar Munirathinam • Petr Král • Rohit Kolhatkar

Received: 23 March 2014 / Accepted: 2 July 2014 / Published online: 5 August 2014

ABSTRACT

Purpose An oligonucleotide termed 'T-oligo' having sequence homology with telomere overhang has shown cytotoxicity in multiple cancers. We have demonstrated that T-oligo can induce apoptosis in androgen independent prostate cancer cell line DU-145. In this report, we evaluate the use of star-shaped tetraspermine (SSTS) for delivery of T-oligo.

Methods SSTS was synthesized from spermine and its intrinsic cytotoxicity towards DU-145 cells was compared with spermine and branched polyethyleneimine (bPEI). Atomistic molecular dynamic (MD) simulations were conducted to understand binding and complexation of spermine and SSTS with T-oligo. Complexation was also determined using gel electrophoresis and SYBR gold assay. Complexes were characterized for size, cellular uptake and antiproliferative effect.

Results SSTS exhibited significantly lower toxicity than spermine and bPEI. Its affinity towards T-oligo was significantly higher than spermine as determined by experimental studies and confirmed by MD simulations and it formed stable complexes (TONPs) with T-oligo. TONPs facilitated cellular uptake and nuclear accumulation of T-oligo and their cytotoxic potential was observed at concentration several folds lower than that required for T-oligo alone.

Conclusion SSTS significantly enhanced therapeutic benefits associated with the use of T-oligo and can be developed as a delivery vehicle for its *in-vivo* therapeutic applications.

KEY WORDS cationic polymers · nucleic acid delivery · oligospermines · T-oligo

ABBREVIATIONS

6-FAM	6-carboxyfluorescein
BCA	Bicinchoninic acid
bPEI	Polyethylenimine, branched
CRPC	Castration resistant prostate cancer
DAPI	4′,6-Diamidino-2-Phenylindole, Dihydrochloride
$EDTA(ONP)_4$	Ethylenediaminetetrakis-(p-nitrophenyl) ester
SSTS	Star-shaped tetraspermine
TONPs	T-oligo nanoplexes

INTRODUCTION

Prostate cancer is the second leading cause of cancer death in men with an estimated 233,000 new cases in the U.S. in 2014 [1]. Although most advanced prostate cancer patients respond initially to androgen deprivation therapy, they stop responding between one and three years after initiation of therapy [2], thus becoming castration resistant. Therefore, new treatments are being investigated to treat castration resistant prostate cancer (CRPC).

Electronic supplementary material The online version of this article (doi:10.1007/s11095-014-1455-7) contains supplementary material, which is available to authorized users.

V. Kolhatkar • H. Khambati • A. Lote • P. Shanine • R. Kolhatkar (✉)
Department of Biopharmaceutical Sciences, University of Illinois Chicago
1601 Parkview Ave, Rm N302, Rockford, Illinois 61107, USA
e-mail: rohitk@uic.edu

G. Munirathinam • R. Kolhatkar
Department of Biomedical Sciences, College of Medicine
University of Illinois Chicago, Rockford, Illinois 61107, USA

T. Insley • S. Sen • P. Král
Department of Chemistry, University of Illinois at Chicago
Chicago, Illinois 60607, USA

P. Král
Department of Physics, University of Illinois at Chicago
Chicago, Illinois 60607, USA

Telomeres are heterochromatic structures present at the ends of linear chromosome and are essential for ensuring chromosome stability [3]. Exposure of telomere overhang induces apoptosis or senescence depending on the type of cancer cell. Exogenous administration of oligonucleotide homologous to the telomere overhang also elicits effects similar to the exposure of telomere overhang [4–6]. One such oligonucleotide termed 'T-oligo'(11-mer), having sequence homology to telomere overhang, exhibits cytostatic and/or cytotoxic effects in multiple cancer cell types while sparing normal primary cells including mammalian epithelial cells [7–10]. Recently, we have demonstrated that T-oligo can inhibit growth of prostate cancer cell line DU-145 lacking androgen receptors [11]. Rankin *et al.* have also reported similar observations [12], thus suggesting its potential in the CRPC treatment. However, in general, oligonucleotides such as T-oligo are poorly internalized owing to their polyanionic character and degrade rapidly in the presence of nucleases [13, 14]. The use of suitable carrier can overcome these limitations associated with the administration of free T-oligo. An ideal carrier can pack the oligonucleotide into nanoparticulate form, protect it from degradation during circulation, and enhance its cellular internalization [15–18].

Cationic polymers are currently investigated as nucleic acid carriers because they can form complexes with negatively charged oligonucleotides through electrostatic interactions [19, 20]. Flexibility of chemistries, facile manufacturing, and robust and stable formulation are some advantages associated with cationic polymers that can ease their transition to clinics. Several cationic polymers have been explored so far as carriers for nucleic acids (antisense oligonucleotides, siRNA and plasmid DNA) [21–24]. But identification of a suitable polycationic polymer with lower intrinsic toxicity and higher transfection remains a challenge. Molecular weight and surface charge are two important factors responsible for the toxicity of polycationic polymers [25, 26]. An increase in molecular weight or surface positive charge increases the cytotoxicity associated with polymers; whereas, relatively small molecular weight polycationic compounds (1-5 K) exhibit lower toxicity [27, 28]. Thus, we want to develop small molecular weight polycationic compounds with lower toxicity profiles, while maintaining their ability to bind to nucleic acids to form complexes within the nanometer size range. Our recent studies demonstrate the potential of spermine-based molecules for nucleic acid delivery [29]. In this manuscript we report the benefits of using star-shaped tetraspermine (SSTS) comprising of four spermine units conjugated to the central core (Fig. 1) as a carrier for T-oligo. We use atomistic molecular dynamics (MD) simulations to examine the binding of spermine and SSTS with T-oligo. We also demonstrate that complexes made of T-oligo and SSTS exhibit antiproliferative properties at much lower concentration than free T-oligo.

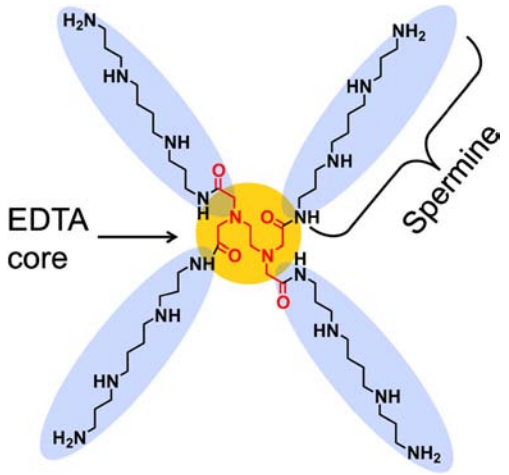

Fig. 1 Schematic representation of star-shaped tetraspermines (SSTS).

MATERIALS AND METHODS

Materials

Spermine (*N*,*N*'-Bis-(3-amino-propyl)-butane-1,4-diamine) was purchased from Alfa Aesar (Ward Hill, MA). DNA oligonucleotides T-oligo 5′ - GTTAGGGTTAG - 3′, the control oligo 5′ - CTAACCCTAAC- 3′ and FAM labeled T-oligo 5′ – (6-FAM)GTTAGGGTTAG - 3′ were purchased from The Midland Certified Reagent Company (Midland, TX). SYBR Gold reagent was obtained from Life Technologies (Grand Island, NY). All other chemicals were obtained from Sigma Aldrich (Milwaukee, WI). All commercial reagents and anhydrous solvents were used without further purification or distillation. High-performance liquid chromatography (HPLC) grade solvents were purchased from Fisher Scientific (Pittsburgh, PA). RPMI 1640 media, PBS, trypsin, antimycotic were purchased from GIBCO (Invitrogen; Grand Island, NY). FBS was purchased from Atlanta biological (Lawrence, GA 30043). DAPI and WST-1 reagent was purchased from Roche Diagnostics (Indianapolis, IN). To study cellular uptake and subcellular trafficking, experiments were performed using 8-chambered slide BD Biosciences Discovery Labware (Bedford, MA). All small molecules were analyzed using TLC, NMR, MS and HPLC for the purity. Thin layer chromatography was performed on Whatman silica gel 60 Å with fluorescent indicator (Partisil K6F). Compounds were visualized by UV light and/or stained with ninhydrin solution followed by heating. Flash column chromatography was performed on Whatman silica gel 60 Å (230–400 mesh). Proton NMR spectra were recorded on a Bruker 400 MHz spectrometer. ESI mode mass spectra were recorded on a Shimatzu LCMS-2020. MALDI analysis was performed using a Voyager-DE PRO mass spectrometer (Applied Biosystems, Foster City, CA) equipped with a 337 nm pulsed nitrogen laser. Gel electrophoresis was performed using BioRad vertical

electrophoresis system Power Pac 200 (BioRadHercules, CA) and bands were visualized using the molecular imager, Chemidoc^{TM} XRS + with image lab software (Bio-Rad Hercules, CA). Polyplex size was measured by a dynamic light scattering spectrophotometer, NICOMP 3802 LS, Santa Barbara, CA.

Methods

Chemistry

Spermine (1) was converted to monoprotected bis-bocspermine (MPBBS) (5) in four steps as shown in Scheme 1. Details of the synthetic procedure are provided in supplementary information. Central core with four amine-reactive arms ethylenediaminetetrakis-(p-nitrophenyl) ester) (6) (EDTA(ONP)$_4$) was synthesized as described previously [30]. SSTS was synthesized by reacting MPBBS (5) with (EDTA(ONP)$_4$) (6) as depicted in Scheme 2. Conjugation of monoprotected bis-bocspermine (5) to the central core (6) yielded *N*-protected form of SSTS. Deprotection of primary amines under basic conditions followed by deprotection of secondary amines under acidic conditions yielded SSTS as trifluoroacetate salt. Detailed procedure about the synthesis is described below.

Synthesis of N-Protected SSTS (7). To the solution of 5 (0.47 g, 0.77 mmol) in 15 mL anhydrous tetrahydrofuran was added N,N-Diisopropylethylamine (2.24 mL, 12.9 mmol) and 6 (0.1 g, 0.13 mmol). Reaction mixture was stirred under nitrogen at room temperature for 24 h. THF was then evaporated and the reaction crude was dissolved in 200 mL dichloromethane, and the organic layer was washed with 0.1 N NaOH (3×50 mL), water (2×50 mL), 1 M $KHSO_4$ (3×50 mL) and water (2×50 mL). Dichloromethane was dried over anhydrous sodium sulfate and evaporated under vacuum to give a yellow oily concentrate. Concentrate was purified by flash column chromatography over silica gel using ethyl acetate:methanol:NH_4OH (70:27:3) as an eluent to afford 0.14 g (48.8%) of compound 7.

Synthesis of Star-Shaped Tetraspermine (SSTS) (8). Compound 7 (0.14 g, 0.063 mmol) was dissolved in a 1:1 mixture of MeOH/NH_4OH (30% aq solution) and refluxed overnight. Then the solvent was evaporated under vacuum. The residue obtained was dissolved in methanol and precipitated in ether to obtain 0.08 g (70%) of pale yellow sticky precipitate of 8, which was found to be pure by TLC and MS analysis. It was used without further purification for the next step. The precipitate 8 (0.08 g, 0.044 mmole) was dissolved in 10 mL 20% solution of trifluoroacetic acid in dichloromethane. The reaction mixture was stirred at room temperature for 2 h. After this time, solvents were evaporated the crude mixture was dissolved in minimum amount of methanol and precipitated in cold ether to obtain 0.09 g, (0.03 mmole, 83%) of SSTS (9) as trifluoroacetate salt. ^{1}H NMR (400 MHz) DMSO-d_6 δ 1.6 (16H, bs, $HNCH_2$-C$\underline{H}_2$-CH_2NH), 1.68–1.82 (8H, m, $HNCH_2$-C$\underline{H}_2$-CH_2NH_2), 1.84–2.0 (8H, m, $CONHCH_2$-C$\underline{H}_2$-CH_2NH), 2.75–3.05 (44H, m, $CH_2C\underline{H}_2NH_2$, $CH_2C\underline{H}_2NH$, $CH_2C\underline{H}_2N$), 3.1–3.2 (8H, m, $CONHC\underline{H}_2CH_2$), 3.45 (8H, m, $COC\underline{H}_2N$), 8.0 (12H, bs, NH_3), 8.4 (4H, bs, CON$\underline{H}$), 8.9 (16H, bd, $CH_2N\underline{H}$); MS Mol. Wt. Calculated (1,029.54) Mol. Wt. Observed (1,030.54, M + 1). SSTS was further characterized using Matrix Assisted Laser Desorption Ionization-Time of Flight mass spectrometry (MALDI-TOF MS) to confirm its molecular weight. SSTS was also characterized using LC/MS to determine the purity and was found to be more than 95% pure. NMR and MALDI spectra of SSTS are shown in Fig. 2.

Preparation and Characterization of T-Oligo Nanoplexes (TONPs)

Stock solutions of 6-FAM-T-oligo (0.08 mM) and SSTS (1.4 mM) were prepared in water. TONPs were formed at varying N/P ratios (0 to 30) by mixing two solutions and final volume was adjusted to 30 μL using water. The solutions were allowed to stand at room temperature for 20 min before analysis. Ability of SSTS to completely complex with T-oligo was examined by monitoring electrophoric mobility of free 6-FAM -T-oligo and TONPs by gel electrophoresis on a BioRad vertical electrophoresis system. Agarose gel (3%, *w/v*)

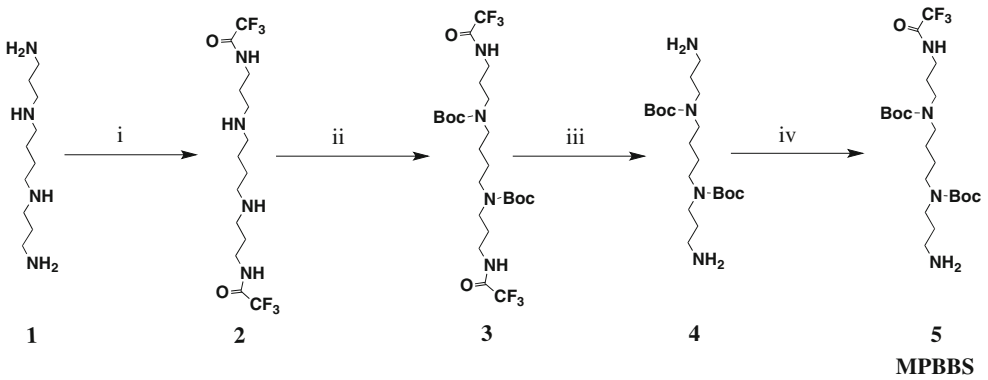

Scheme 1 Synthesis of monoprotected bis-bocspermine i) Ethyl trifluoroacetate ii) Boc anhydride iii) ammonium hydroxide, methanol iv) ethyl trifluoroacetate, −50°C

Scheme 2 Synthesis of star-shaped tetraspermine (SSTS) i) DIPEA; ii) ammonium hydroxide, methanol; iii) TFA

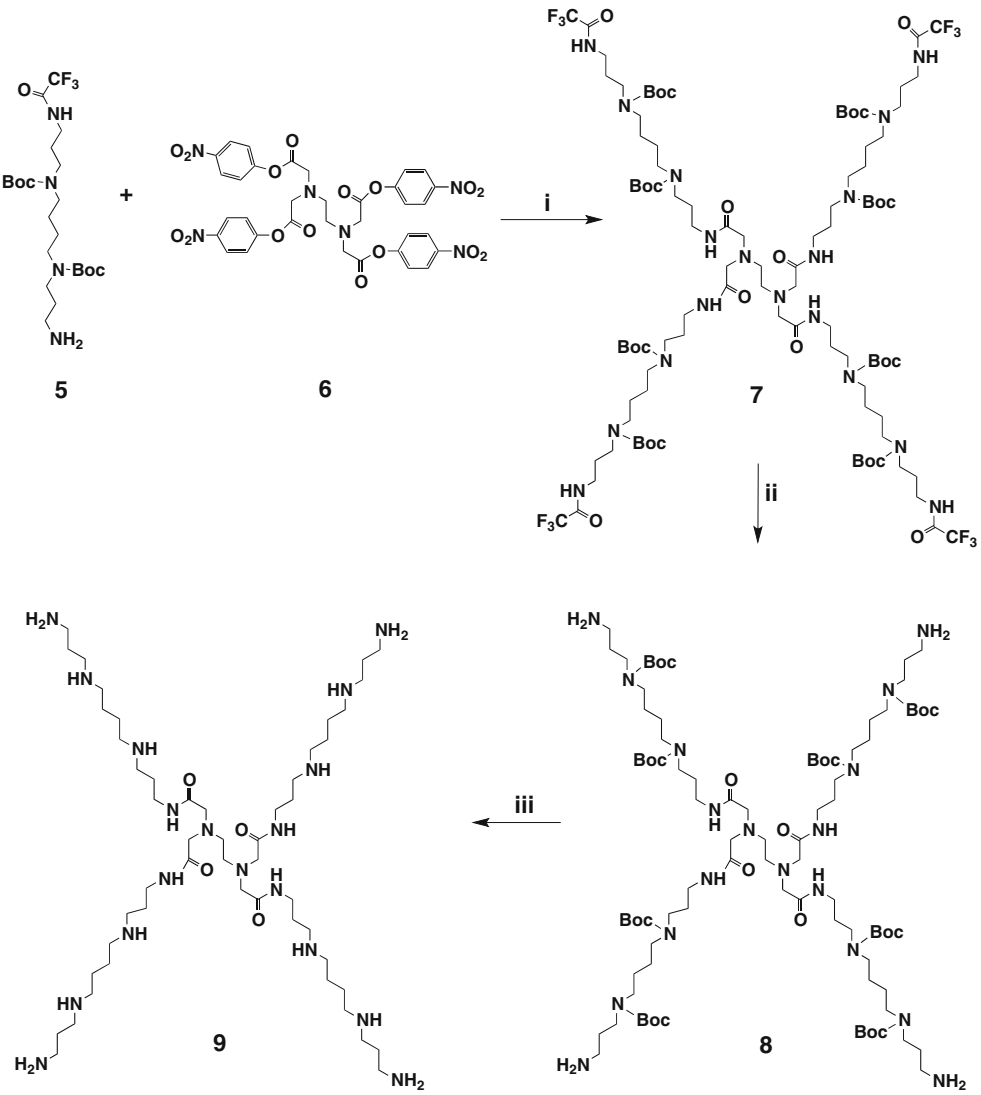

was prepared in 1× TBE (Tris-Boric acid-EDTA) buffer. Ten μL of the TONP solutions (at N/P ratios of 0–30) were mixed with 5 μL of sucrose solution and the mixtures were electrophoresed at 100 V for 20 min. The locations of FAM labeled T-oligo containing bands were visualized by UV illuminator (Fig. 3a). The complex formation and the presence of free T-oligo was also determined by SYBR gold assay as described previously [31] using label free T-oligo. Briefly, 0.5 μg of T-oligo was complexed with SSTS at different N/P ratios in opaque 96 well plates and incubated for 20 min at room temperature. 50 μL of SYBR Gold solution was then added in each well and plate was incubated in dark for 10 min. Intercalation-caused fluorescence was quantified using Synergy 2 multiplate reader (Bio-Tek instruments Winooski, VT) at 495 nm excitation and 537 nm emission wavelengths. Complexation of T-oligo with branched polyethyleneimine (PEI, 25 kD) and spermine was evaluated as well. Experiments were performed in triplicate, and the results are given as mean relative fluorescence intensity values ± standard deviation (Fig. 3b). Intercalation of free T-oligo represents 100% fluorescence and non-intercalating SYBR Gold in buffer represents 0% fluorescence. For size measurement TONPs were prepared as described above. The size of the TONPs was measured in quadruplicates at 25°C using dynamic light scattering spectrophotometer. Results are reported as mean diameter in nm +/− size distribution (Fig. 3c).

Molecular Dynamics Simulations

We modeled the complexation of spermine and SSTS molecules with T-Oligo by atomistic MD simulations using the NAMD package [29] and the CHARMM forcefields par_all27_prot_na.par [32, 33] for T-Oligo nucleotides and cgenff2b7 [34–36] for others. The systems are simulated in the NPT ensemble with periodic boundary conditions applied, using the Langevin dynamics $\gamma_{Lang} = 1.0\ ps^{-1}$. The long range

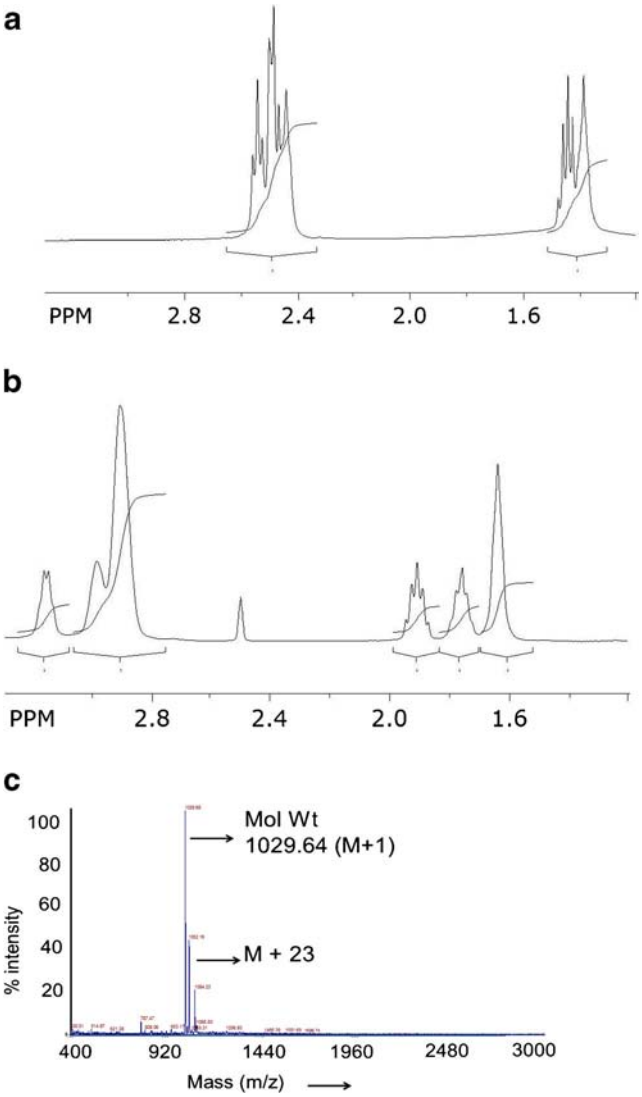

Fig. 2 Characterization of SSTS (**a**) ^{1}H NMR for spermine showing one cluster of peak at 1.5 ppm. (**b**) ^{1}H NMR for SSTS showing three peaks in the region of 1.6–2.0, indicating formation of amide at one end of spermine. (**c**) MALDI analysis indicates one peak (M + 1) corresponding to the molecular weight of SSTS.

electrostatic couplings are calculated by the PME method [37].

In SSTS, we assume that the 12 amines furthest from the EDTA core are protonated giving a +12 net charge. Spermine molecules were given a +3 net charge, so that four spermine molecules would more closely approximate a single SSTS molecule in both mass and charge. We used ammonium and trifluoroacetate counter ions for T-oligo and oligospermines respectively as in the biological experiments. TIP3 water was used as the solvent.

The two primary goals of the simulation studies were to compare the strengths of interaction between spermine and SSTS with T-oligo, and to study in more detail the complexation of SSTS and T-oligo. For this reason three systems were simulated: 1) 1 molecule of T-oligo and 8 molecules of SSTS;

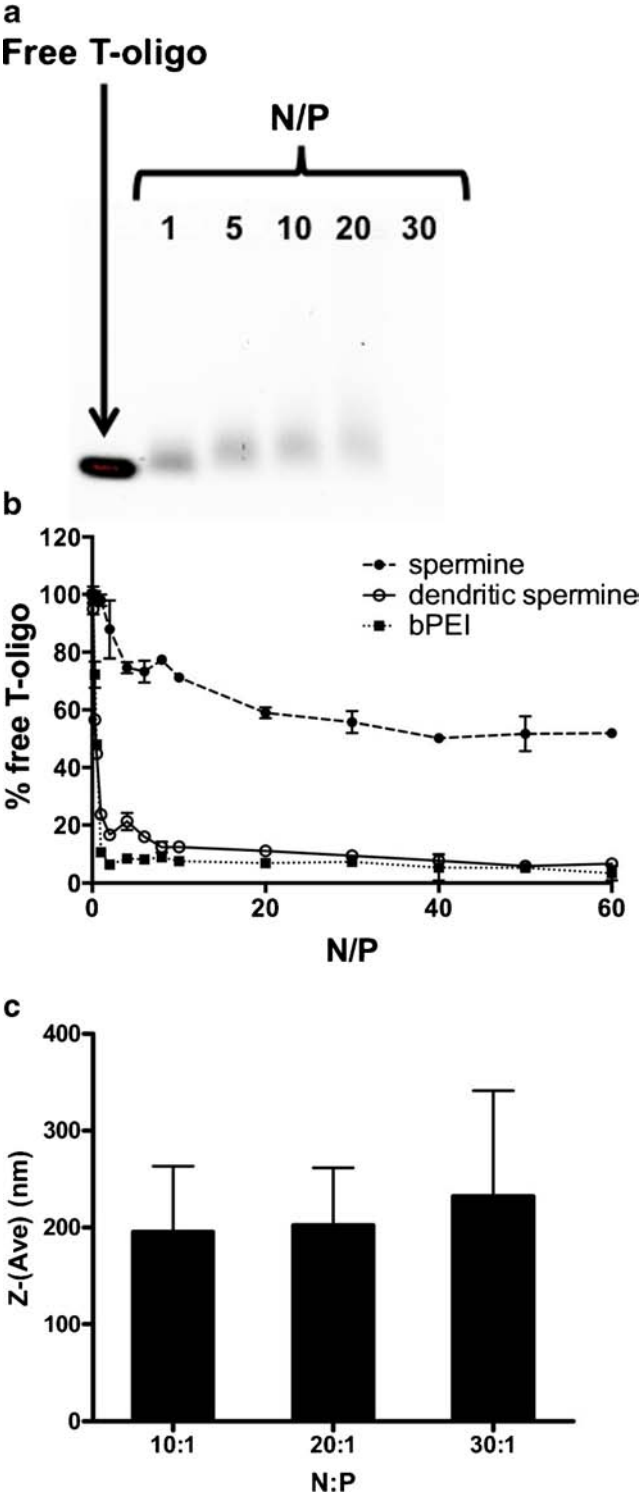

Fig. 3 Characterization of complexes prepared using T-oligo and SSTS. (**a**) TONPs were prepared at different N/P ratios (1, 5, 10, 20, and 30) in water and run on agarose gel. T-oligo band locations were visualized using UV illuminator. Complete complexation was observed when N/P ratio was 30:1 (**b**) Percentage of free T-oligo as detected by SYBR gold assay after complexation with spermine, SSTS and bPEI at different N/P ratios ranging from 0.1 to 60. (**c**) Average diameter of nanoplexes: TONPs were formed at different N/P ratios (10, 20, 30) and size measured by dynamic light scattering spectrophotometer. Error bars represent polydispersity (size distribution) and not the standard deviation. Standard deviation was less than 2%.

2) 1 molecule of T-oligo and 24 molecules of spermine (both were neutralized using ammonium and trifluoroacetate and then solvated in TIP3 water in a $150\times150\times150$ Å^3 periodic bounding box; 24 spermine molecules were used to maintain same N/P ratio as with SSTS); 3) 20 molecules of T-oligo and 150 molecules of SSTS (neutralized by 200 molecules of ammonium and 1,800 molecules of trifluoroacetate and solvated in TIP3 water in a $300\times300\times300$ Å^3 periodic bounding box). All systems were solvated using the VMD solvate plugin. The first and second systems were both equilibrated for 7 ns, the third was equilibrated for 20 ns after using external forces as described below. Complexes obtained from simulations studies are depicted in Fig. 4.

Cell Culture

Androgen independent DU-145 cells were used to measure cellular uptake and growth inhibition. The cells were cultured as previously described [38]. Briefly, cells were cultured in RPMI 1640 media supplemented with 10% of fetal bovine serum (FBS) and 0.5% of antimycotic (the combination of penicillin and streptomycin) at 37°C in 5% CO_2. Cells were passaged after reaching 85–90% confluency.

Cellular Uptake of TONPs

Microscopic Analysis. 6-FAM labeled T-oligo was used to form TONPs to visualize cellular entry and intracellular location of T-oligo and TONPs. DU-145 cells were seeded at a density of 25,000 cells per chamber in 8-chambered slide in 500 µL of complete medium. Cells were incubated for 72 h in presence of 10% serum until they reach 80% confluency. After 72 h, cells were washed twice with complete medium. After washings, the cells were treated with 0.5 mL of 6-FAM-T-oligo or TONPs solutions at various N/P ratios [10, 20, 30] for 1 h, 2 h and 4 h at 37°C. After treatment, cells were washed three times with PBS before observing under fluorescence microscope. To determine nuclear localization DAPI was used as a nuclear stain. At least two independent studies were conducted to visualize internalization of T-oligo and its colocalization with DAPI, and shown in Figs. 5 and 6.

Quantitative Cellular Uptake. Quantitative cellular uptake of 6-FAM labeled T-oligo and TONPs after incubation for 4 and 24 h with DU-145 cells was measured by fluorometry. Treatments were performed as described above. After treatments, cells were washed twice with PBS followed by addition of130µL of 1 N NaOH. Cells were then incubated for 40 min. After incubation, cell lysate was vigorously mixed and 100 µL of cell lysates were transferred to black opaque 96 well plate. Fluorescence was measured at 485 nm excitation and 520 nm emission wavelengths. The data obtained was normalized for protein content, measured using BCA assay. The cellular uptake was compared with bPEI (25 kD) and lipofectamine. Results are depicted in Fig. 7a.

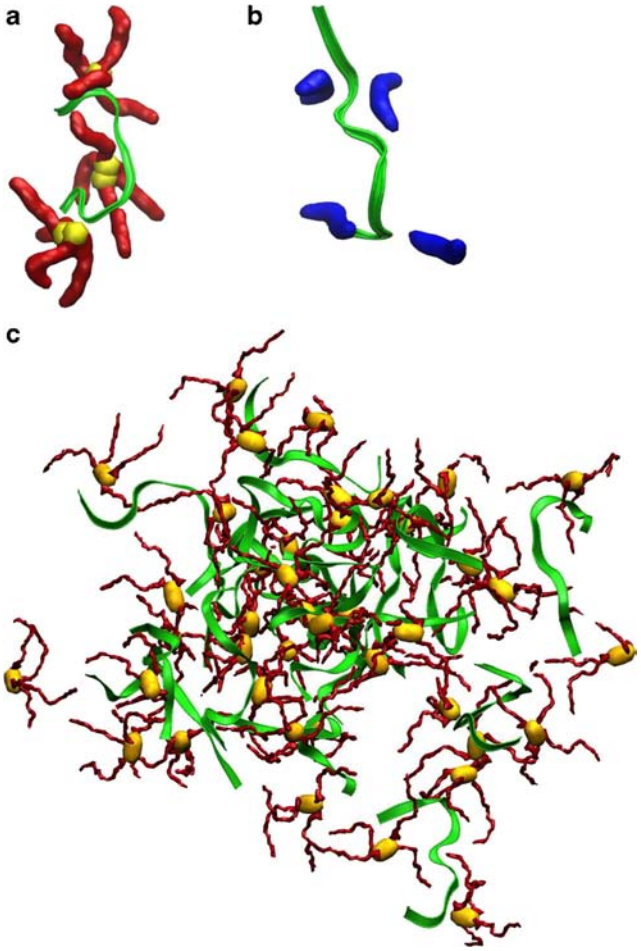

Fig. 4 Complexation of T-oligo with oligospermines (**a**) Small cluster of one T-oligo and three SSTS molecules (**b**) small cluster of one T-oligo and four spermine molecules and (**c**) Big cluster of 20 T-oligo and 42 SSTS molecules. Green ribbons represent T-oligo, red strands with yellow centers represent SSTS molecules, and blue strands represent spermine molecules. Water and counter-ions are not shown.

Fluorescence Assisted Cell Sorting (FACS) Analysis. Uptake mechanism of TONPs in DU-145 cells was investigated as described before for other polycationic systems [39, 40] by using inhibitors of clathrin- and caveolae-mediated endocytosis [41]. DU-145 cells were seeded (100,000 cells/well) in 24 well plate 24 h prior to treatment. Cells were then treated with 200 µL solution of genistein (30 µg/mL) or chlorpromazine (10 µg/mL) or a mixture of genistein and chlorpromazine for 1 h. (These concentrations were found to be non-toxic from cell viability studies conducted separately). Subsequently, TONPs were added at final concentration of 1 µM of 6-FAM-T-oligo in each well and incubation was continued for another 4 h. Media was then aspirated and cells were washed three times with PBS. Trypsin was added to each well and cells

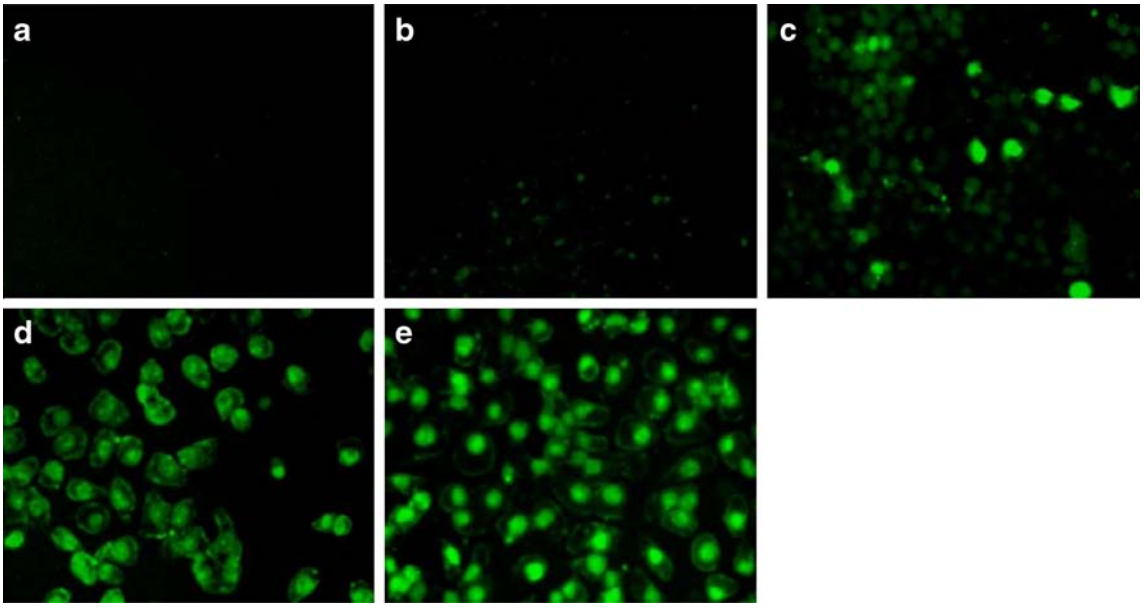

Fig. 5 Intracellular trafficking of TONPs. Fluorescence microscopy images of the DU-145 cell line after incubation at 37°C with (**a**) free T-oligo (10 μM), 1 h or (**b**) TONPs (N/P 20) for 1 h, or (**c**) TONP (N/P 30) for 1 h, or (**d**) TONP (N/P 30) for 2 h or (**e**) TONP (N/P 30) for 4 h. Images in panel (**a**, **b**, and **c**) were captured with 10× lens and in panel (**d**) and (**e**) were captured with 20× lens.

were harvested, mixed with complete media and centrifuged at 5,000 rpm for 4 min. Cell pellets were resuspended in 500 μL complete media and analyzed for the presence of 6-FAM-labeled T-oligo by flow cytometer (Becton Dickinson, Franklin Lakes, NJ) and data analyzed by CellQuest software.

In Vitro Growth Inhibition

Growth inhibition effect and GI_{50} values for free spermine, SSTS, and bPEI (25 kD) were evaluated on DU-145 cells. DU-145 cells (2,000/well for 5 days and 4,000/well for 4 h, 24 h and 48 h treatment) were seeded in 96-wells plate in complete medium for 24 h prior to treatment. On the day of the treatment (day 0), cells were treated with the test substance for predetermined time (4, 24, 48 h or 5 days). At the end of treatments, media was aspirated followed by addition of 110 μL of WST-1 solution. After 4 h, absorbance was measured at 440 nm. Cell growth inhibition was calculated using following formula.

$$\%\ \textit{Growth Inhibition} = \frac{A_T - A_0}{A_C - A_0} \times 100$$

A_T Absorbance of treated cells (at the end of the treatment period)
A_C Absorbance of control cells (at the end of the treatment period)
A_0 Absorbance at Day 0 (Start of the treatment)

Briefly, cell viability at day 0 (start of the treatment) was subtracted from the cell viability after treatment and expressed as percentage growth inhibition compared to untreated cells (Fig. 8). Negative growth inhibition values indicate cell killing. Experiments were routinely conducted in the exponential growth phase. GI_{50} values were determined by nonlinear regression analysis using GraphPadPrism software. Averages of GI_{50} values are reported in Table I for at least two independent experiments performed in triplicate. Similar experiments were performed to determine growth inhibition properties of free T-oligo, control oligo, TONPs and complexes prepared using SSTS of control oligo (Fig. 9, Table II). Cell viability of DU-145 cells after treatment with endocytosis inhibitors (chlorpromazine and genistein) for 5 h was evaluated using similar method to determine non-toxic concentrations for uptake studies.

RESULTS

Synthesis and Characterization of SSTS and TONPs

We have previously described the procedure for the synthesis of the central core with four reactive ester groups [42]. The presence of only one free primary amine in MPBBS [5] facilitated the conjugation of four spermines to the central core. The presence of several Boc groups facilitated the purification of protected form of SSTS using flash column chromatography. Reaction for deprotection of Boc groups after column purification was clean yielding pure SSTS in the TFA salt form. Comparison of NMR spectra for spermine and SSTS revealed

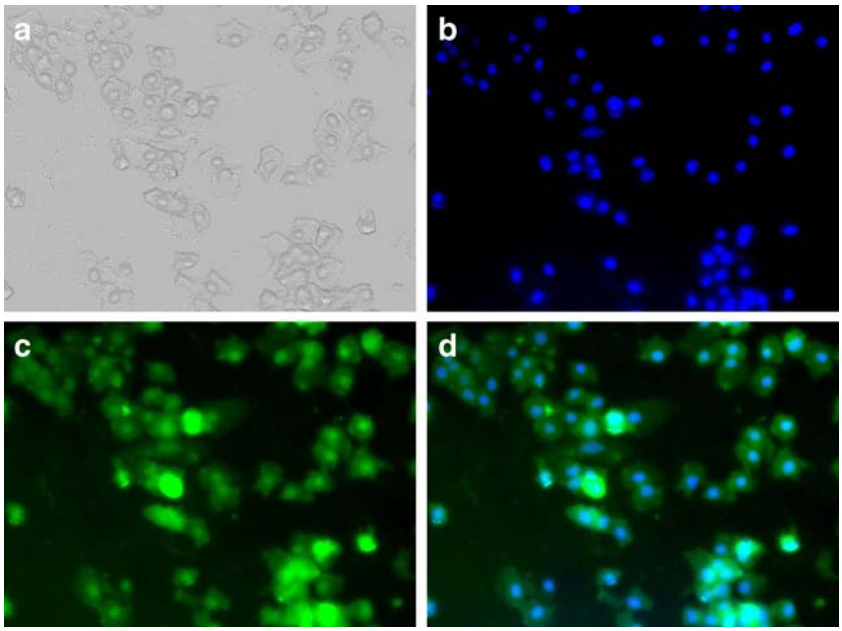

Fig. 6 Fluorescence microscopy images demonstrating nuclear accumulation of FAM-T-oligo in DU-145 cell cells incubated at 37°C with TONP (N/P = 30) for 4 h. (**a**) Light microscope image (**b**) Visualization of nuclear staining by DAPI (**c**) Visualization of FAM-T-oligo and (**d**) Colocalization of DAPI and FAM-T-oligo.

a downfield shift for protons attached to the α-carbon with respect to the primary amine in spermine (Fig. 2a, b). Protons at the β-position to the primary amine (two protons at each end of spermine) appeared as one cluster in spermine NMR, whereas, in SSTS two different peaks were observed due to the formation of amide bond only at one end (Fig. 2a, b). MALDI (Fig. 2c) and MS analysis confirmed molecular weight while LC/MS revealed more than 95% purity for SSTS. To determine buffering capacity, spermine, SSTS, and bPEI were titrated using HCl solution. Titration curves and buffering capacity with respect to pH are plotted, and the graphs are included in supplementary information (Fig S1 and S2). All polyamines (spermine, SSTS and bPEI) exhibited buffering effect at higher pH values (pH > 7) corresponding to their higher pK_a values. Buffering capacity for the change in pH from 7.4 to 5.1 was calculated and reported in Table I. Branched PEI exhibited highest buffering capacity, which was 3.7-folds more than NaCl. Spermine and SSTS showed 2.6- and 2-folds increase in buffering capacity compared to NaCl solution.

Preparation and Characterization of T-Oligonanoplexes (TONPs)

Figure 3a shows the scan of electrophoresis gel for the complexes prepared using SSTS and T-oligo. Lane one is for free T-oligo while lanes 2 to 6 are for complexes at different N/P ratios. Despite the same amount of T-oligo used for complex formation, a decrease in the intensity of the band for free T-oligo was observed with increasing amount of polymer (increasing N/P ratio). The decrease was quite significant even at N/P ratio of one (Lane 2). No free T-oligo was observed at N/P ratio of 30 (Lane 6, Fig. 3a) indicating complete complexation of T-oligo. SYBR gold assay revealed very low percentage of T-oligo in the free form even at low N/P ratios and the percentage of free form remained more or less same at higher N/P ratios. The size of TONPs was measured at 25°C using dynamic light scattering spectrophotometer. The average size for TONPs at N/P ratio 10, 20 and 30 was 195, 202 and 232 nm respectively (Fig. 3c). Since complete complexation was seen at higher N/P ratios, TONPs at N/P ratio of 20 and 30 were used for biological evaluation.

Molecular Dynamics Simulations

We used atomistic MD simulations to compare the strengths of binding between spermine/SSTS and T-oligo, and to study the complexation between T-oligo and SSTS. The Coulombic coupling energy was calculated every 0.004 ns and averaged over 0.4 ns. In Fig. 4a, b, we show the SSTS-T-oligo complex and the spermine-T-oligo complex, respectively. Using VMD [43], we found that in these two complexes the average Coulombic coupling is −202.05 kcal/mol and −117.56 kcal/mol per SSTS and spermine molecules, respectively. These results are in good agreement with the experiments.

In Fig. 4c, we also present the formation of large SSTS-T-oligo complexes. Local complexation occurred first, where small clusters comprising of one molecule of T-oligo and two/three molecules of SSTS were observed to form, in analogy to Fig. 4a. These local complexes then assembled into larger clusters. In order to speed up this process of cluster assembly, we initially applied a small force of 0.69 pN, pulling

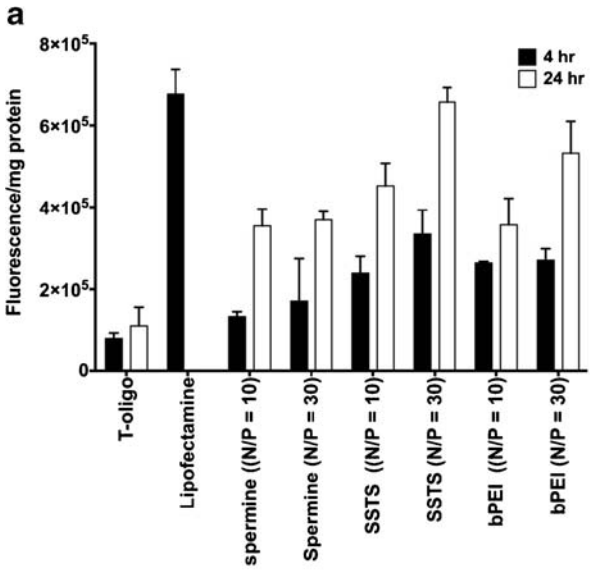

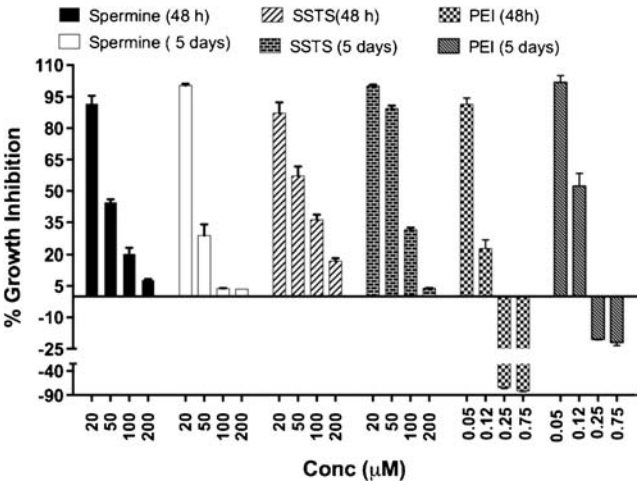

Fig. 8 Cytotoxicity of spermine, SSTS and bPEI (25 kD) after incubation with DU-145 cells for the indicated time period.

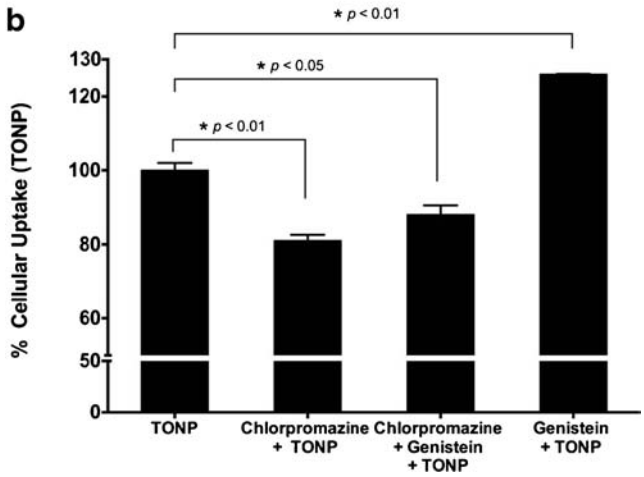

Fig. 7 (**a**) Quantitative measurement of cellular uptake of free FAM labeled T-oligo, spermine-T-oligo complexes, TONPs, and PEI-T-oligo complexes after incubation for 4 h and 24 h with DU-145 cells. Spermine, SSTS, and bPEI significantly enhanced cellular uptake of T-oligo after 24 h incubation compared to free T-oligo. (**b**) DU-145 cells were pre-incubated for 1 h with Chlorpromazine (10 μg/mL), or Genistein (30 μg/mL), or their mixture followed by addition of TONPs. Cellular uptake of TONPs was measured using FACS after 4 h incubation.

the components close to each other. The formed cluster is comprised of 20 T-oligo molecules and 42 SSTS molecules (Fig. 4c). The strong electrostatic attraction between positively charged SSTS molecules and negatively charged T-oligo makes the cluster compact and stable.

Intracellular Trafficking and Quantitative Cellular Uptake of TONPs

To visualize the internalization, TONPs prepared using fluorescently labeled T-oligo (6-FAM T-oligo) were incubated with DU-145 cell lines at 37°C at two different N/P ratios (N/P=20 and 30), and results were compared with free T-oligo. Figure 5a–c shows images from fluorescence microscopy after incubation of free T-oligo, TONP (N/P=20) and TONP (N/P=30) for 1 h. No cellular uptake (Fig. 5a) was observed for free T-oligo; whereas, a significant amount of green florescence indicated internalization of TONPs (Fig. 5b and c). TONPs with N/P ratio of 30 (Fig. 5c) showed higher internalization than TONPs with N/P ratio of 20 (Fig. 5b). To determine sub-cellular localization, TONPs (N/P=30) were incubated with the cells for 2 and 4 h. After 2 h incubation (Fig. 5d), a dispersed green fluorescence was observed throughout the cytoplasm with a trend towards nuclear accumulation (Fig. 5e). After 4 h, a discrete nuclear accumulation was observed (Fig. 5e). To further confirm nuclear accumulation, a co-localization study was performed using DAPI as nuclear stain. Figure 6 shows images taken from fluorescence microscope after incubation with TONPs (N/P=30) for 4 h. Blue fluorescence corresponding to DAPI (Fig. 6b) and green fluorescence corresponding to T-oligo (Fig. 6c) indicates accumulation of DAPI and T-oligo in the nucleus. This was further confirmed by observation of purple color in co-localization pictures (Fig. 6d). To quantitate cellular internalization, cells were incubated with TONPs, washed with PBS, lysed with NaOH solution and the fluorescence was measured and reported in Fig. 7 after normalization with protein content. We used Lipofectamine as a positive control and bPEI for comparison. As expected, very low cellular uptake was observed for naked T-oligo; whereas, lipofectamine significantly increased T-oligo internalization at 4 h. Complexes formed using linear and bPEI and SSTS demonstrated a significant increase in cellular uptake of T-oligo after 4 h, which was further enhanced after increasing the incubation time to 24 h. Enhancement in the cellular uptake of TONPs was comparable to the enhancement observed after incubation of bPEI-T-oligo complexes.

Table I Characteristics of Spermine, SSTS and bPEI

Compound	Molecular weight	No. of amines/mol	Buffering capacity[a] X 10^7	GI_{50} (μM)			
				4 h	24 h	48 h	5 days
Spermine	202.34	4	6.6	>204	>206	49.1	44.4
SSTS	1,029	14	5.1	>206	>204	66.2	84.2
bPEI	25,000	281	9.2	1.04	0.65	0.06	0.1

[a] Buffering capacity (for change in pH from 7.4 to 5.1) = mol of HCl added/change in pH

To determine the mechanism of cellular uptake, DU-145 cells were pre-incubated with chlorpromazine (clathrin-mediated endocytosis inhibitor) or genistein (caveolae-mediated endocytosis inhibitor) or their mixture for 1 h before adding TONPs. Non-toxic concentrations of chlorpromazine (10 µg/mL) and genistein (30 µg/mL) were selected based on the cytotoxicity profile as determined by WST-1 assay. FACS analysis (Fig. 7b) revealed, a decrease in cellular uptake after pre-incubation with chlorpromazine whereas an increase after pre-incubation with genistein compared to the cellular uptake of TONPs alone. Pre-incubation with a mixture also decreased the cellular uptake.

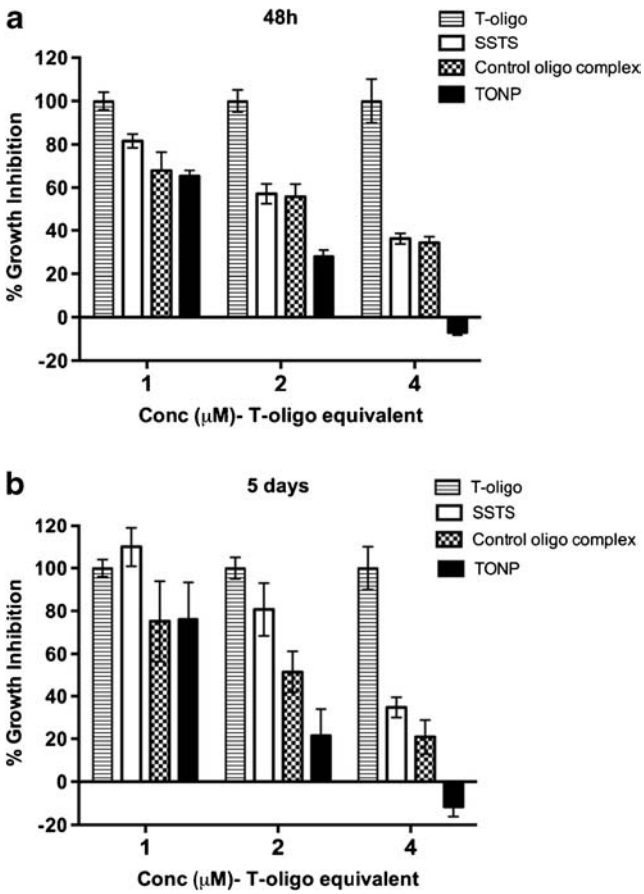

Fig. 9 Cytotoxicity of T-oligo, SSTS, TONPs and control oligonucleotide nanoplexes after incubation with DU-145 cells for (**a**) 48 h and (**b**) 5 days.

Intrinsic Cytotoxicity of Spermine, SSTS and bPEI

Figure 8 illustrates cell viability for spermine, SSTS and bPEI after 48 h and 5 days (GI_{50} values reported in Table I). Cell viability decreased with increase in the concentration and incubation time of spermine and SSTS. No growth inhibition was observed for both compounds at concentrations lower than 0.02 mM (cell viability >90%); whereas, at higher concentrations (0.1 mM) both compounds showed a significant growth inhibition. After 48 h treatment, SSTS, at 0.05 mM and 0.1 mM, was less toxic (cell viability 57 and 36%) than spermine (cell viability 45 and 20%). The difference in cell viability was more pronounced ($p<0.005$) after 5 days of treatment when SSTS treatment showed 89 and 31% cell viability, and spermine treatment showed 29 and 4% cell viability at 0.05 and 0.1 mM respectively. Compared to spermine macromolecules, bPEI was much more toxic. Cytotoxicity of bPEI was more even at the lowest concentration (0.02 mM) tested for SSTS/spermine. Thus, cell viability of bPEI is reported at lower concentrations (Fig. 8). Growth inhibition studies were also conducted at 4 h and 24 h to determine the nontoxic concentrations to be used for transfection studies and GI_{50} are reported in Table I.

In-Vitro Growth Inhibition of DU-145 After Incubation With TONPs

To determine the antiproliferative properties, T-oligo was incubated with DU-145 cells at various concentrations ranging from 1 to 40 µM. T-oligo demonstrated significant toxicity only at higher concentrations (20 µM and 40 uM) (data not shown). Lower nontoxic concentrations (1, 2, and 4 µM) of T-

Table II GI_{50} values of SSTS, T-oligo, and TONPs Using DU-145 Cell Line

	GI_{50} (μM)			
	4 h	24 h	48 h	5 d
SSTS	>206	>204	66.2	84.2
T-oligo	–	>4.0	>4.0	>4.0
TONP (N/P = 30)	–	>4.0	2.04	1.15

oligo were chosen for further studies to evaluate the effect of complexation with SSTS. Cell viabilities of DU-145 after incubation with free T-oligo, free SSTS, TONPs (N/P=30) and complexes prepared from SSTS and control oligo (N/P=30) are reported in Fig. 9 and GI_{50} values are reported in Table II. T-oligo and control oligo when used alone were nontoxic (cell viability >95%) at the concentrations used in these studies. After 48 h treatment (Fig. 9a), a decrease in cell viability was observed for free SSTS at 25, 50, and 100 μM (concentrations required to prepare TONPs at N/P=30 equivalent to 1,2, and 4 μM of T-oligo). Cell viabilities after treatment with nanoplexes prepared from control oligo and SSTS were similar to those after treatment with free SSTS. TONPs were nontoxic at 1 μM (T-oligo equivalent concentration) but exhibited a significant toxicity ($p<0.05$) compared to control oligonanoplexes at 2 and 4 μM (T-oligo equivalent concentrations). After 5 days treatment, the difference in toxicity between TONP and control-oligonanoplexes was more evident at 4 μM. Comparison of GI_{50} values revealed that the toxicity of TONPs was approximately 2-fold higher than control-oligonanoplexes.

DISCUSSION

The objective of this study was to develop a carrier for T-oligo that can facilitate its further development as a therapeutic oligonucleotide. Relatively small size of this oligonucleotide compared to other nucleic acids such as siRNA or plasmid DNA prompted us to develop small molecules different from other polymeric systems currently under investigation as nucleic acid carriers. We chose spermine to use as a building block for SSTS because of its affinity towards nucleic acids. Spermine is an organic cation present at millimolar concentration in eukaryotic cells. At physiological pH, the amine groups in spermine are protonated, enabling them to interact with negatively charged cellular components such as DNA, RNA, and anionic phospholipids [44]. Spermine is known to produce condensed DNA through the interaction of the positively charged amines with the phosphate groups on the nucleosides [45, 46]. Spermine is an important component in several non-viral delivery vectors. It is used to form synthetic cationic lipids that can be assembled to form liposomes. Spermine is also grafted on polysaccharides and other polymers (dextran, chitosan, methacrylate) to achieve the required binding with negatively charged phosphate groups [47–51]. Recent reports indicate higher transfection efficiency for polymers made from spermine (polyspermine) [52–54]. The buffering capacity of polyspermine was better than bPEI, suggesting that the use of spermine in non-viral delivery vectors can lead to the endosomal escape of the carrier-oligonucleotide complex [52]. Efforts from the laboratory of Drs. Smith and Pack demonstrate the potential of spermine dendrons as nucleic acid carriers [55, 56]. We intend to develop spermine-based macromolecules as nucleic acid carriers. Recently, we reported that tetraspermines can successfully knockdown reporter gene expression. Thus, in this study we evaluate the use of SSTS comprising of four spermines conjugated to a central core. SSTS can be considered as generation 0 dendritic spermine with the potential to form higher generation dendritic analogs. The four surface amine groups on SSTS can be branched out to form higher generation dendritic spermine. The synthetic strategy involving conjugation of monoprotected bis-bocspermine to the central core yielded a good amount of tetraspermine, and the presence of Boc groups facilitated the purification of the protected form. Deprotection of primary and secondary amines were high yielding reactions allowing us to synthesize SSTS in pure form in good quantities despite its highly polar nature.

First, we studied the binding of SSTS with T-oligo. Gel retardation assay (Fig. 3a) and SYBR gold assay (Fig. 3b) confirmed complex formation as well as absence of free T-oligo at higher N/P ratios. A complete binding was observed at N/P ratio of 30, which is equivalent to wt/wt ratio of 7:1 (SSTS:T-oligo). Dynamic light scattering analysis revealed sizes of 195, 202 and 232 nm for the complexes formed at 10,20 and 30 N/P ratio.

The MD simulations showed that SSTS has about twice larger binding affinity to T-oligo than spermine. These results support the experimental findings that SSTS binds to T-oligo more strongly than spermine as shown in Fig. 3b. Figure 4a, b reveal that spermine and SSTS bind to T-oligo quite differently. The EDTA core of SSTS lies close to the T-oligo backbone, with one or two legs bound to the DNA and the other two pointing away, which gives only twice larger binding strength compared to spermine despite the fact that SSTS is four times more charged than spermine. In contrast, spermine binds more completely with the DNA strand, with a greater percentage of amines per molecule coupled to the T-oligo. However, SSTS can better neutralize T-oligo than spermine, due to both enthalpic and entropic reasons.

In Fig. 4c, we can see that the loose SSTS arms exposed to the solvent can couple several SSTS-T-oligo complexes into a larger cluster. The strong binding of SSTS is important to keep the complexes stable in the presence of buffer. The loose SSTS arms form a protective barrier for the larger clusters. Pavan *et al.* has reported a similar screening effect when they studied the interaction between spermine dendrons and DNA [57]. Moreover, the non-interacting arms of SSTS could keep the complex positively charged, which can facilitate its cellular uptake. This can perhaps explain higher cellular uptake observed with TONPs than complexes formed with spermine, despite the same N/P ratio used for complexation (Fig. 7a).

The differences in the complexation behavior of spermine and SSTS are also helpful in the development of targeted

delivery systems. Since higher percentage of amines in spermine are engaged in binding to nucleic acid, it is expected that functionalization of these amines will lead to loss in binding energy, whereas loose SSTS arms in TONPs can be functionalized with tumor targeting agents without affecting the stability of the complexes. Additionally, SSTS (Fig. 4a) leaves much less of the DNA backbone exposed compared to the spermine complex (Fig. 4b). By steric interactions this may help prevent nuclease degradation of T-oligo, possibly improving the longevity of the TONPs. These findings suggest that SSTS is perhaps benefiting from its dendritic architecture.

Then, we evaluated intrinsic toxicity of SSTS using androgen independent prostate cancer cell line DU-145. As expected from its molecular weight, cytotoxicity of SSTS was hundreds of fold lower compared to bPEI (Fig. 8, Table I). Spermine dendrons are also reported to be nontoxic at concentrations as high as 20 μg/mL [58]. Reducible polyspermine is also reported to have lower toxicity profile [52]. In agreement with these studies, SSTS was completely nontoxic after 4 h and 24 h incubation period. However, it showed significant toxicity after longer incubation period, albeit only at higher concentrations (Fig. 8).

Previously, we have demonstrated that T-oligo can induce apoptosis in DU-145, a hormone resistant prostate cancer cell line [11]. T-oligo can inhibit growth of DU-145 cell line whereas androgen-dependent cell line LNCaP was unaffected. Rankin *et al.* demonstrated that T-oligo does not generate cytotoxicity, or apoptosis, or cell cycle disruption in normal human prostate epithelial cells (pZ-HPV-7) even after longer exposure time [12]. DU-145 has mutated p53 and pRb suggesting that T-oligo can induce apoptosis even in the absence of p53 and pRb. It is postulated that T-oligo in an unknown manner interferes with the telomeric structure or possibly serving as destabilized telomeric mimic. Therefore, it is essential for T-oligo to reach nucleus, which is its target site. A significant increase in the fluorescence after incubation of complexes as opposed to free T-oligo suggests that SSTS facilitates cellular uptake of T-oligo. Moreover, sufficient incubation period led to the accumulation of green fluorescent in the nucleus. Since fluorescent tag is conjugated to the T-oligo, we speculate that TONPs are either disassembling in the endosomes or disassembling during their transition to nucleus, thus, allowing for nuclear accumulation of T-oligo. Polycationic polymers having higher buffering capacity are expected to facilitate endosomal escape of complexes. Polyspermine has been demonstrated to have significant buffering capacity [52]. However, small molecular weight spermine dendrons require chloroquine for their transfection [59]. Our results reveal a significant fluorescence in cytoplasm at early time points followed by nuclear accumulation after incubation of DU-145 cells with TONPs. These observations suggest the possible escape of complexes during their intracellular trafficking. There is a modest buffering capacity associated with SSTS that might facilitate its endosomal escape. Collectively, both microscopic studies as well quantitative studies suggest higher intracellular concentrations of TONPs compared to free T-oligo validating the importance of delivery system. Quantitative studies further demonstrate that SSTS is equally effective as bPEI and lipofectamine in increasing the cellular uptake of T-oligo. Various reports suggest the involvement of both clathrin and caveolae-meadiated endocytosis for polyplexes prepared from polycationic polymers [39–41, 60, 61]. Thus, we measured the cellular uptake of TONPs after pre-incubation of DU-145 cells with chlorpromazine which is an inhibitor of clathrin-mediated endocytosis and genistein which interferes with caveolae-mediated endocytosis [41]. A modest decrease in the uptake after pre-incubation with chlorpromazine suggests the contribution from clathrin mediated cellular uptake. An increase in the cellular uptake in the presence of genistein may be due to an increased contribution from clathrin-mediated pathway in the absence of caveolae-mediated mechanisms. This is also supported by the fact that a decrease in the uptake was observed by inhibiting both clathrin- and caveolae- mediated pathway (mixture of chlorpromazine and genistein). However, only a modest decrease in the uptake after pre-incubation with mixture also suggests the involvement of clathrin- and caveolae-independent mechanisms.

In-vitro growth inhibition studies demonstrate significantly higher toxicity of TONPs compared to T-oligo. Free T-oligo is cytotoxic to DU-145 cells only at very high concentrations [11]. We have reported a cytotoxic effect of T-oligo at 20 and 40 μM concentration. There was no significant decrease in cell viability at 10 μM. Rankin *et al.* have also reported cytotoxic potential of T-oligo in DU-145 cells at high concentrations [12]. Higher concentrations of T-oligo are also required to generate cytotoxicity in various other cancer cell lines [7, 9]. In this report we demonstrate significant toxicity of T-oligo at 2 and 4 μM when complexed with SSTS. These concentrations are 10–20 fold lower than the concentrations used in previous studies [11, 12]. Roughly, 25 M excess of SSTS is required to achieve complete binding of T-oligo. At such high concentration even SSTS starts showing toxicity. Nevertheless, there is significant difference in the toxicity of TONPs when compared to toxicity of nanoplexes prepared from scrambled oligonucleotide. The difference is more evident at 4 μM and after 5 days treatment. Since SSTS uses spermine as a monomer, there is a possibility that it can interfere with polyamine biosynthesis and metabolism. Although polycationic compounds are expected to disrupt cellular membrane, it is possible that cytotoxicity of SSTS at higher concentration can be related to its interference with the polyamine biosynthesis and metabolism. Oupicky and colleagues have explored and suggested the utility of potent polyamine analog exhibiting higher transfection ability as well

as cytotoxic potential [62]. There is considerable interest in developing polymeric carriers that exhibit some pharmacological activity [63, 64] and SSTS can perhaps behave in a similar fashion. Li *et al*. recently reported the use of bioreducible polycations that not only deliver plasmid DNA, but also inhibit chemokine receptor CXCR4 [65]. It remains to be explored if structural modification of SSTS can lead to the development of a carrier that can interfere with polyamine catabolism and also as a carrier system for nucleic acids.

One of the limitations that we encountered in these studies is higher N/P ratio required for complete binding as well as to enhance cellular internalization. Our simulation studies indicated that this might be due to some of the non-interacting arms present in SSTS. Perhaps more flexibility in the core can lead to higher interaction with nucleic acids as observed with other polymeric systems [66–70]. Our recent observations indicate that increase in the molecular weight of oligospermines increases their binding to nucleic acids. Thus, we anticipate that higher generations of SSTS will be able to form stable complexes at lower N/P ratios. Nevertheless, it was encouraging to observe a significant toxicity of TONPs containing very low concentration of T-oligo, despite an inherently low toxicity associated with T-oligo alone. It is important to emphasize that although T-oligo elicits its pharmacological activity at micromolar concentration, there are several advantages associated with its use. One of them is its selectivity towards cancer cells compared to normal prostate epithelial cells [11, 12]. Another significant advantage associated with the use of T-oligo is its effectiveness in killing androgen-independent prostate cancer cells, which is an important arena that needs to be explored by performing *in-vivo* studies. Use of T-oligo has also been evaluated successfully as an adjuvant therapy in non-Hodkin's-like lymphoma mouse model [5]. Our own findings in this manuscript suggest that use of T-oligo in combination with macromolecules that can interfere with spermine catabolism will be a useful strategy to explore. Future studies in our laboratory will focus on developing TONPs for *in-vivo* applications in an androgen-independent prostate cancer model. We anticipate TONPs to exhibit better pharmacokinetic parameters and tumor accumulation than free T-oligo after *in-vivo* administration. Additionally, functionalizing excess amines present in TONPs by tumor-targeting agents can increase their selectivity towards tumor tissues. Although, this manuscript focuses on the use of T-oligo, SSTS can act as a versatile delivery vehicle. A recent report indicates that deoxyguanosine-enriched T-oligo exhibits higher toxicity compared to T-oligo [12]. Application of SSTS can be extended to this or other highly active oligonucleotides or even siRNAs that are active in nanomolar concentrations. We are currently exploring the possibility of using SSTS as a delivery vehicle for siRNA.

In conclusion, we report a relatively simple and straightforward synthesis of star-shaped tetraspermine (SSTS) that can be used as a delivery vehicle for therapeutic oligonucleotide T-oligo. Future studies will focus on developing TONPs as a treatment modality in androgen-independent prostate cancer mouse model.

ACKNOWLEDGMENTS AND DISCLOSURES

The work was supported by Department of Biopharmaceutical Sciences, College of Pharmacy, University of Illinois at Chicago. Peter Shanine received Riback Fellowship from College of Pharmacy, University of Illinois at Chicago. We also thank Dr. Onyuksel for allowing us to use NICOMP light scattering instrument. Petr Král's work was supported by the NSF-DMR grant No. 1309765 and ACS PRF grant #53062-ND6.

REFERENCES

1. Siegel R, Ma J, Zou Z, Jemal A. Cancer statistics. CA Cancer J Clin. 2014;64:9–29.
2. Cookson MS, Roth BJ, Dahm P, Engstrom C, Freedland SJ, Hussain M, *et al*.. Castration-Resistant Prostate Cancer: AUA Guideline. The Journal of urology. 2013.
3. Martinezand P, Blasco MA. Telomeric and extra-telomeric roles for telomerase and the telomere-binding proteins. Nat Rev Cancer. 2011;11:161–76.
4. Aoki H, Iwado E, Eller MS, Kondo Y, Fujiwara K, Li GZ, *et al*. Telomere 3′ overhang-specific DNA oligonucleotides induce autophagy in malignant glioma cells. FASEB J: Off Publ Fed Am Soc Exp Biol. 2007;21:2918–30.
5. Longe HO, Romesser PB, Rankin AM, Faller DV, Eller MS, Gilchrest BA, *et al*. Telomere homolog oligonucleotides induce apoptosis in malignant but not in normal lymphoid cells: mechanism and therapeutic potential. Int J Cancer J Int du Cancer. 2009;124:473–82.
6. Li GZ, Eller MS, Firoozabadi R, Gilchrest BA. Evidence that exposure of the telomere 3′ overhang sequence induces senescence. Proc Natl Acad Sci U S A. 2003;100:527–31.
7. Sarkarand S, Faller DV. T-oligos inhibit growth and induce apoptosis in human ovarian cancer cells. Oligonucleotides. 2011;21:47–53.
8. Cerone MA, Londoño-Vallejo JA, Autexier C. Telomerase inhibition enhances the response to anticancer drug treatment in human breast cancer cells. Mol Cancer Ther. 2006;5:1669–75.
9. Puri N, Eller MS, Byers HR, Dykstra S, Kubera J, Gilchrest BA. Telomere-based DNA damage responses: a new approach to melanoma. FASEB J: Off Publ Fed Am Soc Exp Biol. 2004;18:1373–81.
10. Yaar M, Eller MS, Panova I, Kubera J, Wee LH, Cowan KH, *et al*. Telomeric DNA induces apoptosis and senescence of human breast carcinoma cells. Breast Cancer Res. 2007;9:R13.
11. Gnanasekar M, Thirugnanam S, Zheng G, Chen A, Ramaswamy K. T-oligo induces apoptosis in advanced prostate cancer cells. Oligonucleotides. 2009;19:287–92.
12. Rankin AM, Forman L, Sarkar S, Faller DV. Enhanced cytotoxicity from deoxyguanosine-enriched T-oligo in prostate cancer cells. Nucleic Acid Ther. 2013;23:311–21.
13. Juliano RL, Ming X, Carver K, Laing B. Cellular Uptake and Intracellular Trafficking of Oligonucleotides: Implications for Oligonucleotide Pharmacology. Nucleic acid therapeutics 2014.
14. Juliano R, Bauman J, Kang H, Ming X. Biological barriers to therapy with antisense and siRNA oligonucleotides. Mol Pharm. 2009;6:686–95.

15. Lee H, Lytton-Jean AK, Chen Y, Love KT, Park AI, Karagiannis ED, *et al.* Molecularly self-assembled nucleic acid nanoparticles for targeted *in vivo* siRNA delivery. Nat Nanotechnol. 2012;7:389–93.
16. Dong Y, Love KT, Dorkin JR, Sirirungruang S, Zhang Y, Chen D, *et al.* Lipopeptide nanoparticles for potent and selective siRNA delivery in rodents and nonhuman primates. Proceedings of the National Academy of Sciences of the United States of America 2014.
17. Zheng M, Pavan GM, Neeb M, Schaper AK, Danani A, Klebe G, *et al.* Targeting the blind spot of polycationic nanocarrier-based siRNA delivery. ACS Nano. 2012;6:9447–54.
18. Scholz C, Kos P, Wagner E. Comb-Like Oligoaminoethane Carriers: Change in Topology Improves pDNA Delivery. Bioconjugate chemistry 2014.
19. Behr JP. Synthetic gene transfer vectors II: back to the future. Acc Chem Res. 2012;45:980–4.
20. Tang MX, Redemann CT, Szoka Jr FC. *In vitro* gene delivery by degraded polyamidoamine dendrimers. Bioconjug Chem. 1996;7: 703–14.
21. Mintzerand MA, Simanek EE. Nonviral vectors for gene delivery. Chem Rev. 2009;109:259–302.
22. Scholzand C, Wagner E. Therapeutic plasmid DNA *versus* siRNA delivery: common and different tasks for synthetic carriers. J Control Release: Off J Control Release Soc. 2012;161:554–65.
23. Alabi C, Vegas A, Anderson D. Attacking the genome: emerging siRNA nanocarriers from concept to clinic. Curr Opin Pharmacol. 2012;12:427–33.
24. Kang HC, Huh KM, Bae YH. Polymeric nucleic acid carriers: current issues and novel design approaches. J Control Release: Off J Control Release Soc. 2012;164:256–64.
25. Merkeland OM, Kissel T. Nonviral pulmonary delivery of siRNA. Acc Chem Res. 2012;45:961–70.
26. Kolhatkar RB, Kitchens KM, Swaan PW, Ghandehari H. Surface acetylation of polyamidoamine (PAMAM) dendrimers decreases cytotoxicity while maintaining membrane permeability. Bioconjug Chem. 2007;18:2054–60.
27. Kunath K, von Harpe A, Fischer D, Petersen H, Bickel U, Voigt K, *et al.* Low-molecular-weight polyethylenimine as a non-viral vector for DNA delivery: comparison of physicochemical properties, transfection efficiency and *in vivo* distribution with high-molecular-weight polyethylenimine. J Control Release: Off J Control Release Soc. 2003;89:113–25.
28. Fischer D, Li Y, Ahlemeyer B, Krieglstein J, Kissel T. *In vitro* cytotoxicity testing of polycations: influence of polymer structure on cell viability and hemolysis. Biomaterials. 2003;24:1121–31.
29. Elsayed M, Corrand V, Kolhatkar V, Xie Y, Kim NH, Kolhatkar R, *et al.* The influence of oligospermine architecture on their suitability for siRNA delivery. Biomacromolecules 2014.
30. Shankar R, Samykutty A, Riggin C, Kannan S, Wenzel U, Kolhatkar R. Cathepsin B degradable star-shaped peptidic macromolecules for delivery of 2-methoxyestradiol. Mol Pharm. 2013;10: 3776–88.
31. Merkel OM, Mintzer MA, Librizzi D, Samsonova O, Dicke T, Sproat B, *et al.* Triazine dendrimers as nonviral vectors for *in vitro* and *in vivo* RNAi: the effects of peripheral groups and core structure on biological activity. Mol Pharm. 2010;7:969–83.
32. Foloppeand N, MacKerell AD. All-atom empirical force field for nucleic acids: I. Parameter optimization based on small molecule and condensed phase macromolecular target data. J Comput Chem. 2000;21:86–104.
33. MacKerelland AD, Banavali NK. All-atom empirical force field for nucleic acids: II. Application to molecular dynamics simulations of DNA and RNA in solution. J Comput Chem. 2000;21:105–20.
34. Vanommeslaeghe K, Hatcher E, Acharya C, Kundu S, Zhong S, Shim J, *et al.* CHARMM general force field: a force field for drug-like molecules compatible with the CHARMM All-atom additive biological force fields. J Comput Chem. 2010;31:671–90.
35. Vanommeslaeghe K, Raman EP, MacKerell AD. Automation of the CHARMM general force field (CGenFF) II: assignment of bonded parameters and partial atomic charges. J Chem Inf Model. 2012;52: 3155–68.
36. Vanommeslaegheand K, MacKerell AD. Automation of the CHARMM general force field (CGenFF) I: bond perception and atom typing. J Chem Inf Model. 2012;52:3144–54.
37. Darden T, York D, Pedersen L. Particle mesh ewald - an N.Log(N) method for ewald sums in large systems. J Chem Phys. 1993;98: 10089–92.
38. Borgman MP, Ray A, Kolhatkar RB, Sausville EA, Burger AM, Ghandehari H. Targetable HPMA copolymer-aminohexylgeldanamycin conjugates for prostate cancer therapy. Pharm Res. 2009;26:1407–18.
39. Rejman J, Bragonzi A, Conese M. Role of clathrin- and caveolae-mediated endocytosis in gene transfer mediated by lipo- and polyplexes. Mol Ther:J Am Soc Gene Ther. 2005;12:468–74.
40. Shi J, Schellinger JG, Johnson RN, Choi JL, Chou B, Anghel EL, *et al.* Influence of histidine incorporation on buffer capacity and gene transfection efficiency of HPMA-co-oligolysine brush polymers. Biomacromolecules. 2013;14:1961–70.
41. Vercauteren D, Vandenbroucke RE, Jones AT, Rejman J, Demeester J, De Smedt SC, *et al.* The use of inhibitors to study endocytic pathways of gene carriers: optimization and pitfalls. Mol Ther:J Am Soc Gene Ther. 2010;18:561–9.
42. Shankar R, Samykutty A, Riggin C, Kannan S, Wenzel U, Kolhatkar R. Cathepsin B Degradable Star Shaped Peptidic Macromolecules for Delivery of 2-methoxyestradiol. Molecular pharmaceutics 2013.
43. Humphrey W, Dalke A, Schulten K. VMD: Visual molecular dynamics. J Mol Graph Model. 1996;14:33–8.
44. Weisell J, Hyvonen MT, Hakkinen MR, Grigorenko NA, Pietila M, Lampinen A, *et al.* Synthesis and biological characterization of novel charge-deficient spermine analogues. J Med Chem. 2010;53:5738–48.
45. Feuerstein BG, Pattabiraman N, Marton LJ. Spermine-DNA interactions: a theoretical study. Proc Natl Acad Sci U S A. 1986;83: 5948–52.
46. Feuerstein BG, Pattabiraman N, Marton LJ. Theoretical models of spermine/DNA interactions. Ann N Y Acad Sci. 1986;482:251–4.
47. Jiang HL, Lim HT, Kim YK, Arote R, Shin JY, Kwon JT, *et al.* Chitosan-graft-spermine as a gene carrier *in vitro* and *in vivo*. Eur J Pharmaceutics and Biopharmaceutics: Off J Arbeitsgemeinschaft fur Pharmazeutische Verfahrenstechnik eV. 2011;77:36–42.
48. Abdullah S, Wendy-Yeo WY, Hosseinkhani H, Hosseinkhani M, Masrawa E, Ramasamy R, *et al.* Gene transfer into the lung by nanoparticle dextran-spermine/plasmid DNA complexes. J Biomed Biotechnol. 2010;2010:284840.
49. Pack DW, Hoffman AS, Pun S, Stayton PS. Design and development of polymers for gene delivery. Nat Rev Drug Discov. 2005;4:581–93.
50. Eliyahu H, Makovitzki A, Azzam T, Zlotkin A, Joseph A, Gazit D, *et al.* Novel dextran-spermine conjugates as transfecting agents: comparing water-soluble and micellar polymers. Gene Ther. 2005;12:494–503.
51. Amini R, Jalilian FA, Abdullah S, Veerakumarasivam A, Hosseinkhani H, Abdulamir AS, *et al.* Dynamics of PEGylated-dextran-spermine nanoparticles for gene delivery to leukemic cells. Appl Biochem Biotechnol. 2013;170:841–53.
52. Jere D, Kim JE, Arote R, Jiang HL, Kim YK, Choi YJ, *et al.* Akt1 silencing efficiencies in lung cancer cells by sh/si/ssiRNA transfection using a reductable polyspermine carrier. Biomaterials. 2009;30: 1635–47.
53. Duan SY, Ge XM, Lu N, Wu F, Yuan W, Jin T. Synthetic polyspermine imidazole-4, 5-amide as an efficient and cytotoxicity-free gene delivery system. Int J Nanomedicine. 2012;7:3813–22.

54. Duan S, Yuan W, Wu F, Jin T. Polyspermine Imidazole-4,5-imine, a Chemically Dynamic and Biologically Responsive Carrier System for Intracellular Delivery of siRNA. Angew Chem Int Ed Engl 2012.
55. Barnard A, Posocco P, Pricl S, Calderon M, Haag R, Hwang ME, *et al.* Degradable self-assembling dendrons for gene delivery: experimental and theoretical insights into the barriers to cellular uptake. J Am Chem Soc. 2011;133:20288–300.
56. Jones SP, Gabrielson NP, Wong CH, Chow HF, Pack DW, Posocco P, *et al.* Hydrophobically modified dendrons: developing structure-activity relationships for DNA binding and gene transfection. Mol Pharm. 2011;8:416–29.
57. Pavan GM, Danani A, Pricl S, Smith DK. Modeling the multivalent recognition between dendritic molecules and DNA: understanding How ligand "sacrifice" and screening Can enhance binding. J Am Chem Soc. 2009;131:9686–94.
58. Jones SP, Pavan GM, Danani A, Pricl S, Smith DK. Quantifying the effect of surface ligands on dendron-DNA interactions: insights into multivalency through a combined experimental and theoretical approach. Chemistry. 2010;16:4519–32.
59. Hardy JG, Kostiainen MA, Smith DK, Gabrielson NP, Pack DW. Dendrons with spermine surface groups as potential building blocks for nonviral vectors in gene therapy. Bioconjug Chem. 2006;17:172–8.
60. Rejman J, Conese M, Hoekstra D. Gene transfer by means of lipo- and polyplexes: role of clathrin and caveolae-mediated endocytosis. J Liposome Res. 2006;16:237–47.
61. Sahay G, Alakhova DY, Kabanov AV. Endocytosis of nanomedicines. J Control Release: Off J Control Release Soc. 2010;145:182–95.
62. Dong Y, Li J, Wu C, Oupicky D. Bisethylnorspermine lipopolyamine as potential delivery vector for combination drug/gene anticancer therapies. Pharm Res. 2010;27:1927–38.
63. Chen Y, Sen J, Bathula SR, Yang Q, Fittipaldi R, Huang L. Novel cationic lipid that delivers siRNA and enhances therapeutic effect in lung cancer cells. Mol Pharm. 2009;6:696–705.
64. Martinand ME, Rice KG. A novel class of intrinsic proteasome inhibitory gene transfer peptides. Bioconjug Chem. 2008;19:370–6.
65. Li J, Zhu Y, Hazeldine ST, Li C, Oupicky D. Dual-function CXCR4 antagonist polyplexes to deliver gene therapy and inhibit cancer cell invasion. Angew Chem Int Ed Engl. 2012;51:8740–3.
66. Sun C, Tang T, Uludag H. Molecular dynamics simulations for complexation of DNA with 2 kDa PEI reveal profound effect of PEI architecture on complexation. J Phys Chem B. 2012;116:2405–13.
67. Pavan GM, Mintzer MA, Simanek EE, Merkel OM, Kissel T, Danani A. Computational insights into the interactions between DNA and siRNA with "rigid" and "flexible" triazine dendrimers. Biomacromolecules. 2010;11:721–30.
68. Pavan GM, Albertazzi L, Danani A. Ability to adapt: different generations of PAMAM dendrimers show different behaviors in binding siRNA. J Phys Chem B. 2010;114:2667–75.
69. Meneksedag-Erol D, Tang T, Uludag H. Molecular modeling of polynucleotide complexes. Biomaterials. 2014;35:7068–76.
70. Elder RM, Emrick T, Jayaraman A. Understanding the effect of polylysine architecture on DNA binding using molecular dynamics simulations. Biomacromolecules. 2011;12:3870–9.